The Earth as a Radio Source: Terrestrial Kilometric Radiation

DONALD A. GURNETT

Department of Physics and Astronomy, University of Iowa, Iowa City, Iowa 52242

Radio wave experiments on the Imp 6 and 8 satellites have shown that the earth emits very intense electromagnetic radiation in the frequency range of about 50–500 kHz. At peak intensity the total power emitted in this frequency range is about 10^9 W. The earth is therefore a very intense planetary radio source, with a total power output comparable to the decametric radio emission from Jupiter. We refer to this radio emission from the earth as terrestrial kilometric radiation. Terrestrial kilometric radiation appears to originate from low altitudes (less than 3.0 R_E) in the auroral region. The intensity of the noise has a pronounced dependence on both the local time and the magnetic latitude of the observing point. At large radial distances the radiation is primarily observed on the poleward side of two cone-shaped surfaces that are centered on the earth and symmetrically located with respect to the northern and southern auroral zones. The magnetic latitude of the cone-shaped boundaries varies from greater than 50° in the local morning to near the magnetic equator in the local evening. Poleward of these boundaries the noise occurs in sporadic 'storms' lasting from ½ hour to several hours. Comparisons with auroral photographs obtained from the low-altitude polar-orbiting Dapp satellite show that the terrestrial kilometric radiation is closely correlated with the occurrence of discrete auroral arcs, which occur in the local evening region of the auroral zone. This association indicates that the kilometric radiation is probably generated by intense 'inverted V' electron precipitation bands, which cause the discrete auroral arcs. Possible mechanisms that can explain the generation and propagation of the terrestrial kilometric radiation are discussed.

Intense electromagnetic radiation is commonly observed propagating outward from the earth in the frequency range of about 50–500 kHz with the University of Iowa plasma wave experiments on the Imp 6 and 8 satellites. Since the wavelength of this radiation is usually in the kilometric range, we shall refer to this radiation as terrestrial kilometric radiation. Terrestrial kilometric radiation was first discovered by *Dunckel et al.* [1970] from very low frequency (VLF) radio measurements with the Ogo 1 satellite. Dunckel et al. refer to this radiation as 'high-pass' noise because the upper frequency of the Ogo VLF receiver (100 kHz) was too low to reach the peak in the emission spectrum. As we shall show, the spectrum of the terrestrial kilometric radiation extends with significant intensities up to about 500 kHz and typically reaches maximum intensity at about 200 kHz. *Brown* [1973] has also commented on observations of earth-related radio emissions at 150–300 kHz with the Goddard Space Flight Center (GSFC) radio astronomy experiment on Imp 6 and refers to this noise as 'midfrequency' radiation.

At peak intensity we will show that the total power of the terrestrial kilometric radiation is about 10^9 W. The earth is therefore a very intense planetary radio source, with a total power output comparable to the decametric (3.0–30.0 MHz) radio emission from Jupiter. For comparison, the total power of the Jovian decametric radiation is estimated by *Warwick* [1963] to be about 2×10^7 W. As we shall also show, the terrestrial kilometric radiation appears to originate from relatively low altitudes (less than 3 R_E) in the auroral regions and is closely correlated with the occurrence of discrete auroral arcs detected optically by the low-altitude polar-orbiting Dapp reconnaissance satellite. Since the maximum energy dissipated by the auroral charged-particle precipitation is about 10^{11} W, the mechanism for generating this radiation must be very efficient (~1%). Because the terrestrial kilometric radiation has many features in common with Jovian, solar, and other astrophysical radio sources, the understanding of this radiation is of considerable general interest, particularly since in this case direct in situ measurements can be made in the source region. The purpose of this paper is to present a comprehensive study of terrestrial kilometric radiation as observed by the Imp 6 and 8 satellites.

INSTRUMENTATION

The Imp 6 spacecraft was launched on March 13, 1971, into a highly eccentric earth orbit with initial perigee and apogee geocentric radial distances of 6613 and 212,630 km, respectively, orbit inclination of 28.7°, and period of 4.18 days. The Imp 8 spacecraft was launched on October 26, 1973, into a slightly eccentric earth orbit with initial perigee and apogee geocentric radial distances of 147,434 and 295,054 km, respectively, orbit inclination of 28.6°, and period of 11.98 days. Both spacecraft are spin-stabilized, their spin axes being oriented very nearly perpendicular to the ecliptic plane.

The University of Iowa plasma wave experiment on Imp 6 is designed to study plasma wave phenomena in the frequency range 20 Hz to 200 kHz. The antennas for this experiment consist of three mutually orthogonal 'long' dipole antennas for electric field measurements and three mutually orthogonal loop antennas for magnetic field measurements. Two of the electric dipole antennas are perpendicular to the spacecraft spin axis. These antennas, E_x and E_y, have tip-to-tip lengths of 53.5 and 92.5 m, respectively. The third electric antenna, E_z, lies along the spin axis and has a tip-to-tip length of 7.7 m. The signals from these antennas are analyzed by two 16-channel spectrum analyzers with center frequencies from 36 Hz to 178 kHz. The filter for each channel has a bandwidth of approximately 15% of the center frequency, and there are four filters per decade of frequency. Each frequency channel has two detectors: a peak detector and an average detector. The peak detector has a response time constant of 0.1 s and measures the largest signal occurring in a given sample interval (5.11 s), and the average detector measures the average noise intensity during the same sample interval. The output of each detector is a voltage proportional to the logarithm of the signal amplitude. The dynamic range of each spectrum analyzer channel is 100 dB. Further details of the Imp 6 plasma wave experiment are given by *Gurnett and Shaw* [1973].

The University of Iowa plasma wave experiment on Imp 8 is similar to the Imp 6 experiment. The antennas for the Imp 8 experiment consist of two orthogonal fine-wire (0.020 inch in diameter) dipole antennas for electric field measurements and three mutually orthogonal search coil magnetometers for magnetic field measurements. The electric dipole antennas are extended outward, perpendicular to the spacecraft spin axis, by centrifugal force. The nominal tip-to-tip length of the electric dipole antennas is 121.8 m. Because of a mechanical failure in one of the antenna extension mechanisms, only the E_y antenna is extended to the full length. All data presented in this report are obtained with the E_y antenna. The spectrum analyzer used in the Imp 8 experiment is very similar to the Imp 6 spectrum analyzer. Fifteen channels are used for electric field measurements covering the frequency range 40 Hz to 178 kHz, there being approximately four channels per decade of frequency. Each channel is sampled once every 10.24 s. In addition to the 15 channel spectrum analyzers the Imp 8 experiment also has a wide-band receiver that can provide wave form measurements over the frequency range 10 Hz to 1 kHz from any selected antenna. The wide-band receiver can also be tuned to frequencies of 2.0 MHz, 500 kHz, 125 kHz, and 31.25 kHz, so that wave form measurements can be obtained at these frequencies. An amplitude output is also available from the wide-band receiver, so that frequency spectrum measurements can be obtained at frequencies up to 2.0 MHz by stepping the center frequency of the wide-band receiver.

OBSERVATIONS

Survey of basic characteristics. An example of terrestrial kilometric radiation observed by Imp 6 is illustrated in Figure 1, which shows the electric field strength in the 178-, 100-, 56.2-, and 31.1-kHz channels for a 24-hour period while the spacecraft is near apogee in the geomagnetic tail region. The ordinate for each frequency channel in this figure is proportional to the logarithm of the electric field strength. The interval from the base line of one channel to the base line of the next higher channel corresponds to a dynamic range of 75 dB. The vertical bars indicate the average field strength over the time interval between samples, and the dot above each bar indicates the peak field strength over this same interval. The distinct enhancements in the 100- and 178-kHz channels of Figure 1, extending as much as 60 dB above the receiver noise level, are typical of the terrestrial kilometric radiation observed by Imp 6. The intensity of this noise often varies considerably (by as much as 20 dB) on a time scale of a few minutes or less. The kilometric radiation occurs in distinct 'storms' lasting for periods from ½ hour to several hours (Figure 1). Between the storms the noise may be completely undetectable, sometimes for periods lasting as long as 24 hours. On a time scale of a minute or less the peak and average field strengths tend to vary together, the typical difference being about 3 dB. As will be shown later, this difference between the peak and the average field strengths is primarily caused by the antenna rotation and indicates that the source has a small angular size as viewed by Imp 6 at large radial distances from the earth.

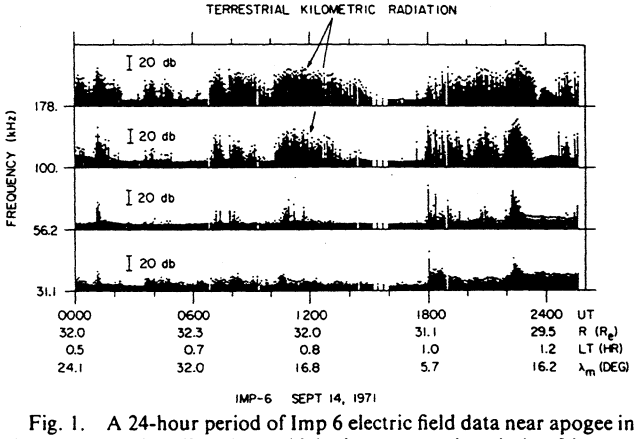

Fig. 1. A 24-hour period of Imp 6 electric field data near apogee in the geomagnetic tail region, which shows several periods of intense terrestrial kilometric radiation in the 100- and 178-kHz channels.

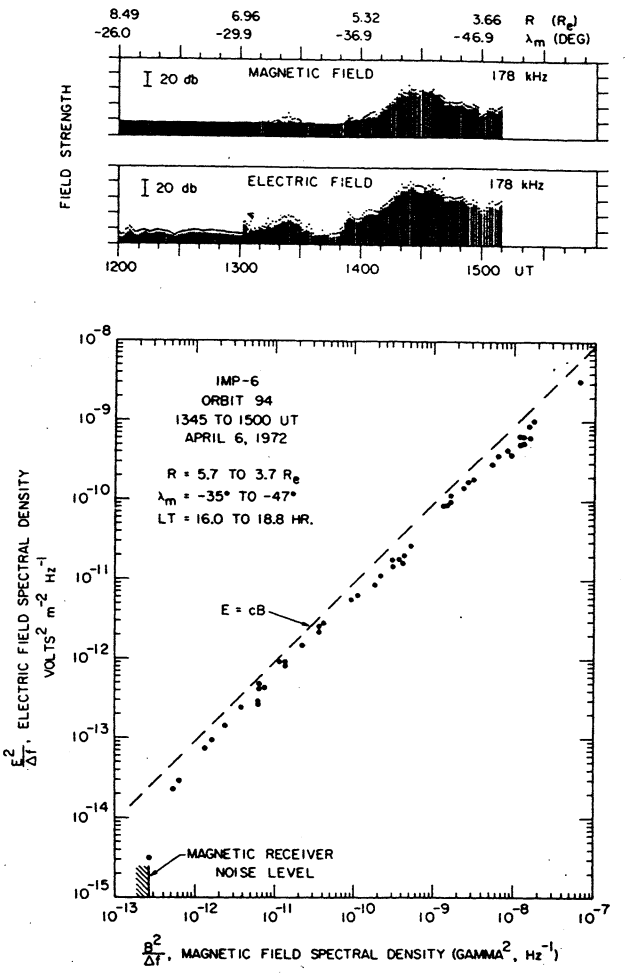

Fig. 2. Simultaneous electric and magnetic field intensities from an inbound Imp 6 pass in the local evening, which show that the terrestrial kilometric radiation consists of electromagnetic waves. The dashed line $E = cB$ gives the electric to magnetic field ratio of an electromagnetic wave in free space.

It is easily shown that the kilometric noise detected by the electric antenna on Imp 6 is electromagnetic radiation, since the same noise is also detected with the magnetic loop antenna on Imp 6. Figure 2 illustrates the electric and magnetic field amplitudes for an intense kilometric noise storm observed during an inbound Imp 6 pass from about 6.0- to 3.7-R_E radial distance. The close correspondence between the electric and the magnetic field amplitudes is clearly evident in the top panel of Figure 2. The bottom panel of Figure 2 shows the corresponding electric and magnetic field spectral densities computed at several points from about 1345 to 1500 UT during this pass. The electric field strength is determined by dividing the measured ac voltage at the antenna terminals by one half

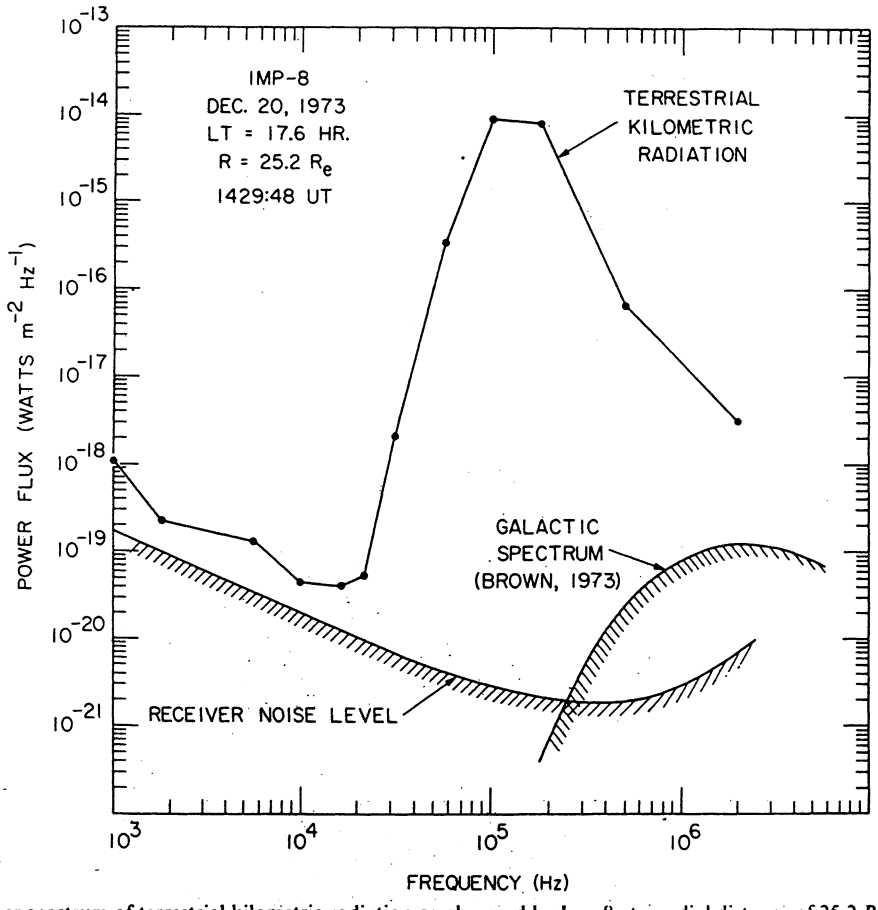

Fig. 3. Power spectrum of terrestrial kilometric radiation as observed by Imp 8 at a radial distance of 25.2 R_E in the local evening.

of the tip-to-tip length of the antenna and ignoring any antenna impedance corrections. The linear relation between the electric and the magnetic field spectral densities illustrated in the bottom panel of Figure 2 provides convincing evidence that the terrestrial kilometric noise detected by Imp 6 is electromagnetic radiation. The small deviation (~20%) of the electric field amplitude from the $E = cB$ line for electromagnetic waves in free space is believed to be due to the loading effect of the input capacity at the base of the electric antenna. The absolute sensitivity of the electric antenna can be directly determined by comparison with the loop antenna response, since no antenna impedance corrections are necessary for the magnetic field measurements.

The frequency spectrum of a typical kilometric noise event is shown in Figure 3. This spectrum was obtained from Imp 8 at a radial distance of about 25.2 R_E in the local evening. The power flux in Figure 3 was computed from the measured electric field spectrum by assuming that the radiation is propagating radially outward from the earth and that both polarizations have equal power. The spectrum in Figure 3 shows the main spectral characteristics of the terrestrial kilometric radiation observed by Imp 6 and 8: (1) the spectrum reaches peak intensity in the range of about 100–300 kHz, (2) the spectrum decreases rapidly with decreasing frequency below about 100 kHz and is seldom detectable at 31.1 kHz, and (3) the spectrum decreases rapidly with increasing frequency above about 300 kHz and is usually down to near the cosmic noise level at 2.0 MHz.

Evidence of near-earth origin. Several characteristics of the terrestrial kilometric radiation indicate that the noise is generated very close to the earth, probably at a radial distance of less than 3 R_E. As was mentioned earlier, the measured intensity of the kilometric noise has a very distinct modulation due to the rotation of the antenna. Figure 4 shows an example

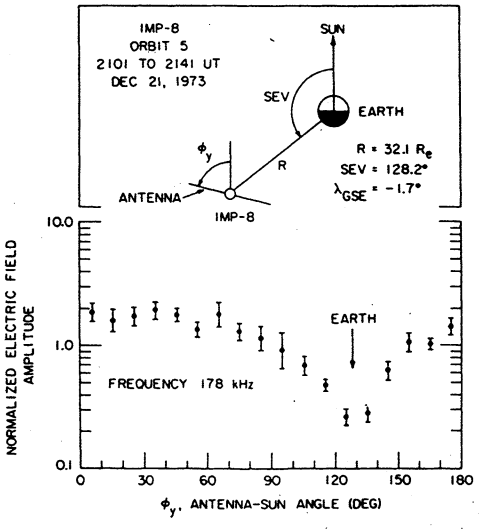

Fig. 4. Angular distribution of the electric field component parallel to the electric antenna axis as a function of the antenna orientation. The deep null when the antenna is pointed at the earth shows that the kilometric radiation appears to be coming from the earth and that the source has a small angular size (<6° half angle) as viewed from Imp 8 at 32.1 R_E.

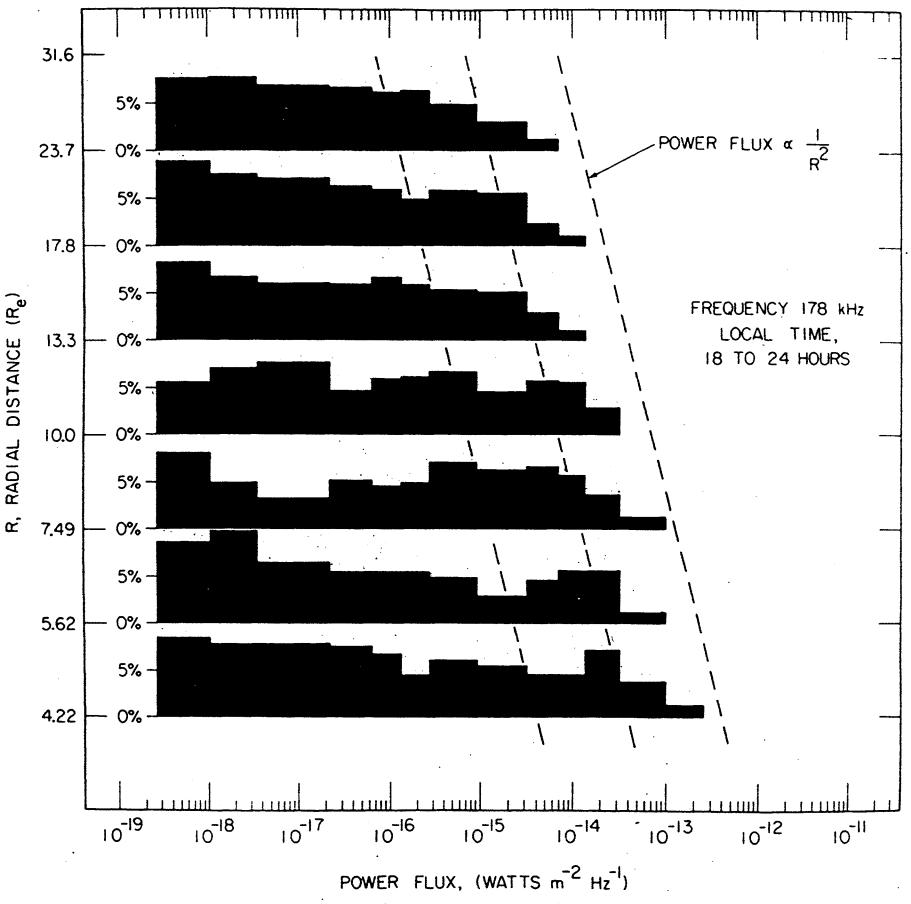

Fig. 5. Power flux distribution of terrestrial kilometric radiation at 178 kHz as a function of radial distance. The radial distance intervals are logarithmically spaced so that a $(1/R)^2$ variation is indicated by a straight dashed line in this diagram.

of spin modulation from the Imp 8 spacecraft. As is indicated in Figure 4, the spacecraft is at a radial distance of about 32.1 R_E in the local evening, and the sun-earth-vehicle (SEV) angle, projected onto the ecliptic plane, is about 128.2°. The geocentric solar ecliptic latitude, $\lambda_{GSE} = -1.7°$, is such that the earth is located very close to the plane of rotation of the antenna, thereby assuring a sharp null for radiation coming directly from the earth.

The antenna orientation angle ϕ_y in Figure 4 is the angle between the electric antenna axis and the spacecraft-sun line. Because of the rapid intensity fluctuations and the slow sampling rate (one sample every 10.24 s) it is necessary to average a large number of measurements to obtain a suitable angular distribution. The amplitudes plotted in Figure 4 are an average of 40 min of data from the 178-kHz channel during a period when intense kilometric noise was being detected. To reduce the error caused by intensity variations, the measured field strengths are blocked into 3.6-min intervals and are normalized by dividing by the average field strength. The normalized electric field amplitudes shown in Figure 4 are the average of the normalized field strengths obtained in each 10° interval from 0° to 180°. Because of the symmetry of the dipole antenna pattern, angles in the range $180° < \phi_y \leq 360°$ are shifted by 180° into the range $0° < \phi_y \leq 180°$.

A null is clearly evident in Figure 4 at an antenna orientation angle of about 130°. This null position corresponds almost exactly to the angular position of the earth (SEV angle of 128.2°). The null is also very deep, the null amplitude being almost a factor of 10 below the peak amplitude. The deep null indicates that the source must have a small angular size, less than about 6° half width, as viewed from Imp 8 at 32.1 R_E. This angular size shows that the source does not extend more than about 3.0 R_E from the center of the earth.

If the source of the kilometric radiation is located close to the earth, then the power flux should vary inversely with the square of the radial distance from the earth. This radial dependence can be verified directly with the Imp 6 data. Figure 5 shows the power flux distribution as a function of radial distance from the earth in the 178-kHz electric field channel. The bar graph within each radial distance interval gives the percentage occurrence of the kilometric noise as a function of the power flux within that range of radial distances. These percentage occurrences are computed by using all data points (327.6-s averages) obtained during 1 year of in-flight operation totaling 22,802 measurements. To reduce the effect of local time variations, only local times in the range 18–24 hours are considered. All points are included without regard to the type of noise being detected. From the 24-hour survey plots, such as that shown in Figure 1, we have established that virtually all of the noise detected in the 178-kHz channel consists of terrestrial kilometric radiation. The radial distance ranges in Figure 5 are logarithmically spaced so that a $(1/R)^2$ dependence of the power flux is a straight line in this diagram. The peak power flux is seen to follow closely the $(1/R)^2$ dependence indicated by the dashed lines in Figure 5, thereby providing further evidence of the near-earth origin of the kilometric radiation. The data in Figure 5 also provide quantitative information on the intensity of the kilometric radiation at any given radial dis-

tance. At a radial distance of 30 R_E the maximum intensity is about 10^{-14} W m^{-2} Hz^{-1} at 178 kHz.

Spatial distribution of the radiation. In addition to the $(1/R)^2$ radial variation the kilometric radiation also has a pronounced dependence on the local time and the latitude of the observing point. The local time dependence is illustrated in Figure 6, which shows the local time and radial distance coordinates of Imp 6 for times when the power flux in the 178-kHz channel exceeds a threshold power flux of

$$\text{threshold} = \left(\frac{R_E}{R}\right)^2 \times (7.35 \times 10^{-16}) \text{ W m}^{-2} \text{ Hz}^{-1}.$$

The $(1/R)^2$ factor in the threshold for counting an event is to correct for the expected $(1/R)^2$ variation of the power flux with radial distance. This threshold corresponds to a power flux of 8.16×10^{-19} W m^{-2} Hz^{-1} at $R = 30\ R_E$, which is much less than the average power flux of the kilometric radiation, so that essentially all events that occur should be detected. The data in Figure 6 represent 1 complete year of in-flight operation, thereby assuring coverage of all local times. In order to provide an unbiased representation the time interval between points in Figure 6 is adjusted to give a constant number of samples per unit length along the trajectory.

Figure 6 shows that the kilometric radiation is much more frequently observed in the local evening (from about 16.0 to 4.0 hours local time) than in the local morning. The noise is seldom observed from about 6.0 to 12.0 hours local time. Figure 6 also shows a sharp cutoff in the kilometric radiation at a radial distance of about 3.0 R_E at all local times. The location of this cutoff (near the expected location of the plasmapause boundary) suggests that the plasmasphere is affecting the propagation of the kilometric radiation in this region.

To investigate this plasmapause effect further, the frequency of occurrence has been determined as a function of the magnetic latitude and radial distance in the local time range 18.0–24.0 hours, where the noise is most frequently observed. Magnetic latitude λ_m is used as a parameter because the plasmasphere is known to be controlled strongly by the geomagnetic field. To correct for the expected $(1/R)^2$ variation of the power flux, the threshold for counting an event is again varied as

$$\text{threshold} = \left(\frac{R_E}{R}\right)^2 \times (7.35 \times 10^{-16}) \text{ W m}^{-2} \text{ Hz}^{-1}$$

Data from 2 years of in-flight operation are used to determine the frequency of occurrence. Because of the limitations imposed by the Imp 6 orbit it is necessary to combine the northern hemisphere and southern hemisphere data, the sign of the magnetic latitude being ignored, in order to obtain an adequate number of samples in each λ_m, R block. The percentage occurrences computed from these data are shown in Figure 7. All latitudes below the upper border marked 'limit of latitudinal coverage' have at least 20 samples in each λ_m, R block. A well-defined low-latitude cutoff in the occurrence of kilometric radiation is evident in Figure 7, varying from about 40° magnetic latitude at 3.0 R_E to about 10° magnetic latitude at 10.0 R_E. At radial distances of less than about 4.0 R_E this

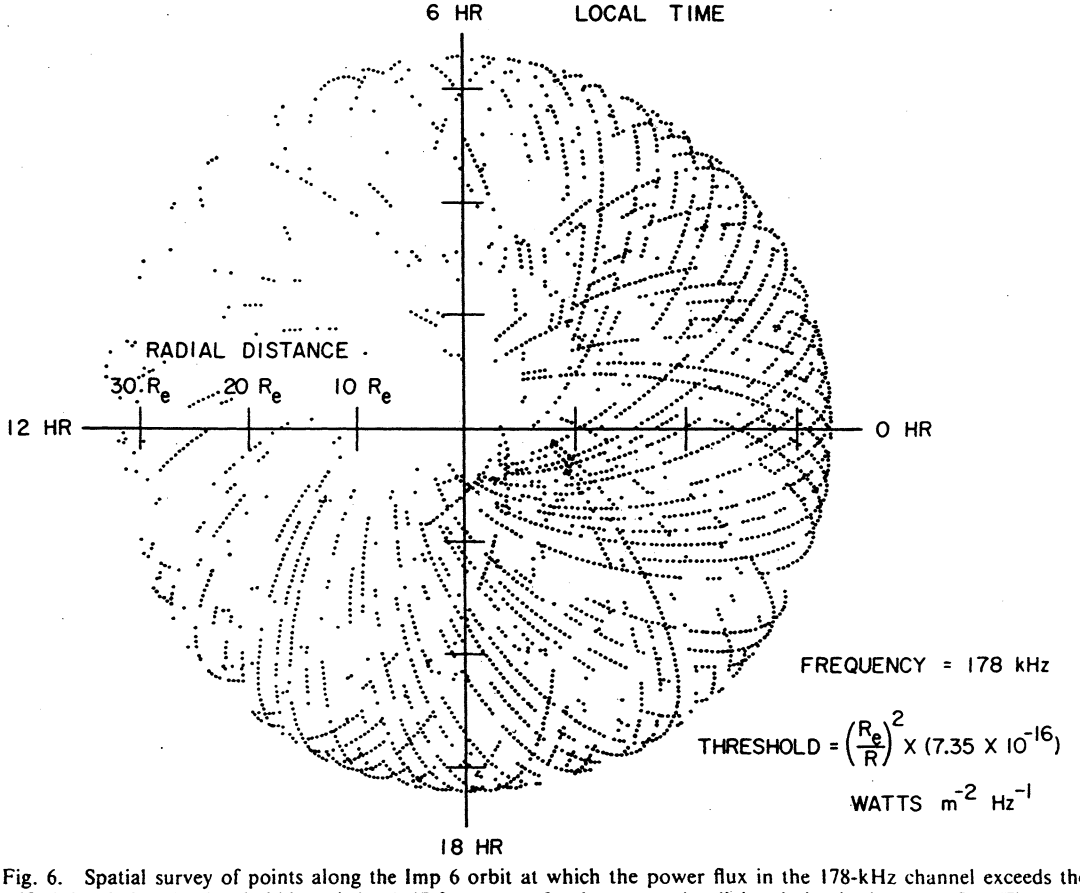

Fig. 6. Spatial survey of points along the Imp 6 orbit at which the power flux in the 178-kHz channel exceeds the specified threshold. The threshold is varied as $(1/R)^2$ to correct for the expected radial variation in the power flux. The coordinates are geocentric radial distance and local time.

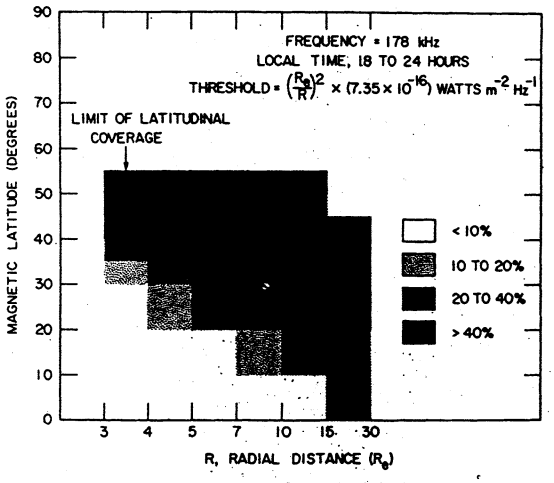

Fig. 7. Percentage occurrence of terrestrial kilometric radiation as a function of magnetic latitude and radial distance. Again the threshold is varied as $(1/R)^2$ to correct for the expected radial variation in the power flux. Note the shadow zone extending from about 40° magnetic latitude at 3.0 R_E to about 10° magnetic latitude at 10.0 R_E.

cutoff coincides closely with the rapid increase in the plasma density that occurs at the plasmapause. Figure 8 shows a low-altitude Imp 6 pass selected to illustrate this cutoff at the plasmapause. The plasmapause in this case was identified from the abrupt change in the low-frequency (<300 Hz) electric field interference generated by the spacecraft solar array (see the discussion by *Gurnett and Shaw* [1973]). Figure 8 shows that the kilometric radiation detected during this pass disappears abruptly as the spacecraft crosses the plasmapause at 1913 UT. This abrupt termination is believed to be due to a propagation cutoff that occurs when the plasma frequency f_p exceeds the wave frequency as the spacecraft enters the plasmasphere. Note in Figure 8 that the cutoff in the 100-kHz channel (at 1913 UT) occurs before the cutoff in the 178-kHz channel (at 1918 UT). This sequence of cutoffs is consistent with the expected rapid increase in the plasma density and plasma frequency as the spacecraft passes into the plasmasphere.

The systematic difference between the peak (dots) and average (bars) intensities of the kilometric radiation observed during the inbound low-altitude pass in Figure 8 indicates that a significant amount of spin modulation (30% null-to-peak ratio) still exists even at radial distances as close as 2.8 R_E, thereby implying that the source of the radiation still subtends a small angular size even at this low altitude. These results indicate that the kilometric radiation must originate from the high-latitude low-altitude regions of the magnetosphere. The Imp 6 spacecraft probably does not pass through the source region, since as is evident in Figure 8, the orbit does not provide high-latitude ($\lambda_m > 50°$) measurements at radial distances of less than about 3.0 R_E.

At higher altitudes (greater than about 4.0 R_E) the low-latitude cutoff of the kilometric radiation is not as abrupt as the example shown in Figure 8, and the cutoff does not correspond with the local plasmapause location. As is shown by Figure 7, there appears to be a 'shadow zone' near the magnetic equator extending out to radial distances of about 10–15 R_E. The existence of this shadow zone is further confirmed by the fact that terrestrial kilometric radiation is almost never detected by the University of Iowa plasma wave experiment on the S³-A satellite, which has an orbit near the magnetic equator even though the spacecraft often crosses into the region beyond the plasmapause to radial distances of 5.24 R_E.

To determine the angular distribution of the kilometric radiation, as would be observed far from the earth, the frequency of occurrence has also been determined as a function of magnetic local time (MLT) and magnetic latitude. Magnetic coordinates are used because of the expected geomagnetic control of the source. To avoid effects due to the propagation cutoff at the plasmapause, we have used only measurements obtained at radial distances greater than 5 R_E. The threshold for counting events is again varied according to the relation

$$\text{threshold} = \left(\frac{R_E}{R}\right)^2 \times (7.35 \times 10^{-16})\ \text{W}^2\ \text{m}^{-2}\ \text{Hz}^{-1}$$

to correct for the expected variation in the power flux with radial distance. The results of this investigation, using 2 years of Imp 6 data from the 178-kHz channel, are shown in Figure 9. The limits of the latitudinal coverage provided by Imp 6 are indicated by the solid lines at the outer boundaries of the shaded region in this diagram.

The frequency-of-occurrence contours in Figure 9 show that in the northern hemisphere the kilometric radiation is confined to a single region with a distinct cone-shaped equatorward boundary. A similar region with a cone-shaped equatorward boundary is also evident in the southern hemisphere. Near local midnight the two cone-shaped boundaries appear to merge, and the radiation is detected at all magnetic latitudes sampled by Imp 6, although there is a reduced frequency of occurrence near the magnetic equator. On the day side of the earth (from about 6.0 to 12.0 hours MLT) the radiation is observed only at very high magnetic latitudes: $\lambda_m > 45°$ in the northern hemisphere and $\lambda_m < -45°$ in the southern

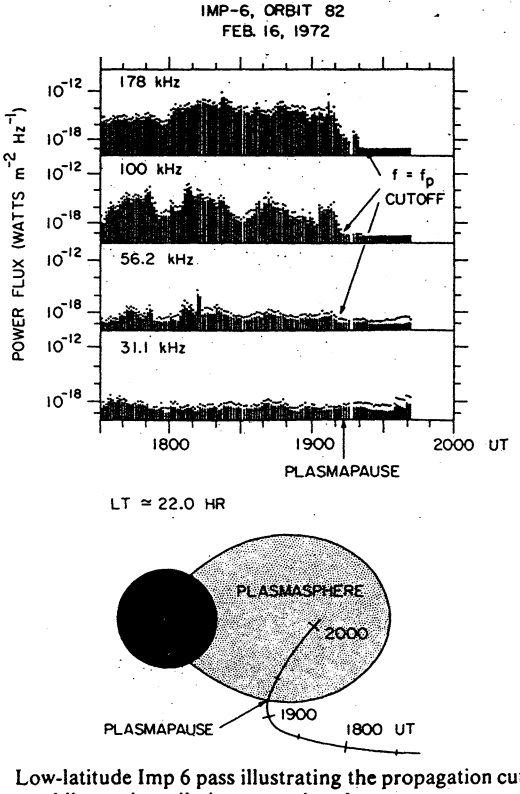

Fig. 8. Low-latitude Imp 6 pass illustrating the propagation cutoff of kilometric radiation near the plasmapause.

hemisphere. In the local midnight region the frequency of occurrence does not show any tendency to decrease at high latitudes. From about 12 to 20 hours MLT, however, a distinct latitudinal maximum exists in the frequency of occurrence, varying in location from about $\lambda_m = 30°$ at 20 hours MLT to about $\lambda_m = 45°$ at 12 hours MLT. This latitudinal maximum suggests that a poleward minimum probably exists in the frequency of occurrence over the polar cap regions.

CORRELATION WITH AURORA

Because the terrestrial kilometric radiation appears to be coming from low altitudes in the auroral zone, we have investigated the relationship of this radio noise to the occurrence of aurora by using auroral photographs from the U.S. Air Force Dapp satellite. The Dapp spacecraft is in a sun-synchronous dawn-dusk polar orbit at an altitude of 830 km. An optical scanner on the spacecraft provides a synoptic view of almost the entire nighttime auroral oval on each polar pass. It is found that the occurrence of intense kilometric radiation is closely associated with the occurrence of aurora. This conclusion is based on a study of about 150 Dapp auroral photographs (one photograph per orbit) obtained during January 1973. Because of the difficulty in providing a quantitative auroral index from the Dapp photographs the results of this study are qualitative. Whenever a bright extensive auroral display occurs in the Dapp photographs, intense kilometric radiation is always detected by Imp 6 if the spacecraft is located in a favorable region for receiving this radiation. When no auroral light is evident, the kilometric radiation is usually weak or undetectable.

To illustrate the observed relationship between the aurora and the kilometric radiation, a particular day, January 25, 1973, has been selected for discussion. This day was selected both because this day is representative of the relationships observed during other periods and because the Dapp auroral photographs for this day have previously been published by *Snyder et al.* [1974] and are available for comparison. Figure 10 shows the envelope of the ground magnetogram records (*H* component) for this day and the power flux in the 178-kHz channel of Imp 6. The difference between the upper and the lower magnetogram envelopes in Figure 10 is the auroral electrojet index *AE*, frequently used as a measure of auroral substorm activity.

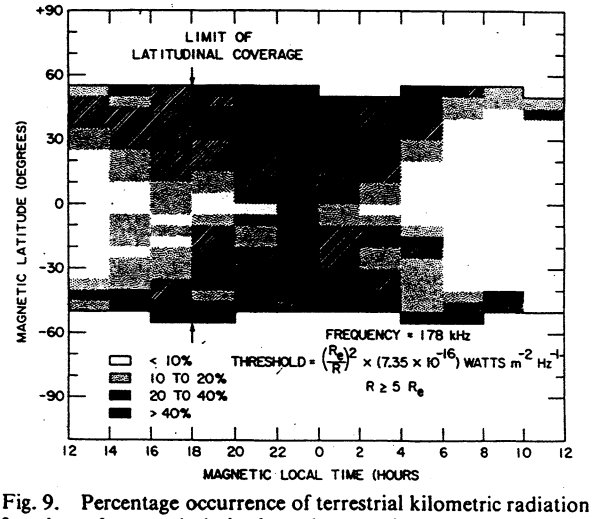

Fig. 9. Percentage occurrence of terrestrial kilometric radiation as a function of magnetic latitude and magnetic local time. Again the threshold is varied as $(1/R)^2$ to correct for the expected radial variation in the power flux. Note the cone-shaped equatorward boundary of the emission regions in the northern and southern hemispheres.

The only significant activity evident in the Dapp photographs from 0000 to 1000 UT occurs on orbit 1089 (see the paper by *Snyder et al.* [1974] for the Dapp photograph from this orbit). The aurora observed during orbit 1089 is associated with the weak magnetic activity from about 0200 to 0400 UT, and a corresponding small enhancement in the 178-kHz power flux is evident in Figure 10.

The first major auroral substorm activity on January 25, 1973, starts at about 1000 UT. The Dapp auroral photographs obtained during this substorm are shown in Figure 11. The magnetic pole in each of these photographs is located near the top center of the photograph, dusk being on the left and dawn on the right (see the paper by *Snyder et al.* [1974] for further details). The photograph for orbit 1093, which was taken at about 0940 UT (before the onset of the substorm), shows essentially no auroral activity. No kilometric radiation is detected in the 178-kHz channel at this time. The next photograph, that for orbit 1094, which was taken at about 1125 UT (near the time of maximum magnetic disturbance), shows an extensive region of bright auroral light emission extending along the entire auroral oval from dawn to dusk. Several bright arcs, called discrete auroras, are evident on the poleward boundary of the auroral oval extending from local early evening, in the upper left-hand corner, around to local midnight in an almost continuous band. In the local midnight region, equatorward of the discrete arcs, a broad band of diffuse aurora is also evident extending beyond the lower edge of the photograph. The bottom panel of Figure 10 shows that very intense kilometric radiation ($\sim 5 \times 10^{-13}$ W m^{-2} Hz^{-1}) is observed by Imp 6 simultaneous with the auroral light emissions observed by Dapp on orbit 1094. On the following Dapp photograph, taken on orbit 1095, the discrete arcs have completely disappeared, and the 178-kHz kilometric radiation has correspondingly disappeared. A small band of diffuse aurora, however, is still seen near the lower edge of the photograph.

The second major substorm activity on January 25, 1973, starts at about 1330 UT. The next Dapp photograph, that for orbit 1096, which was taken at about 1440 UT, again occurs near the time of maximum magnetic activity, and an extensive region of bright auroral light emission is evident. Figure 10 shows that again, in association with the aurora, very intense kilometric radiation ($\sim 3 \times 10^{-14}$ W m^{-2} Hz^{-1}) is observed by Imp 6. On the next Dapp orbit, 1097, the kilometric radiation has decreased to near the receiver noise level, and the auroral photograph for this orbit shows that the aurora has correspondingly disappeared.

The third major auroral substorm activity on January 25, 1973, starts at about 1950 UT. The Dapp photographs obtained during this substorm are shown in Figure 12. The photograph for Dapp orbit 1099, which was taken at about 1805 UT (before the onset of the substorm), shows no significant auroral activity, and no kilometric radiation is detectable by Imp 6 at this time. The next photograph, that for Dapp orbit 1099, which was taken at about 1955 UT (during the period of increasing magnetic activity associated with the expansive phase of the substorm), shows a small bright discrete arc in the local evening. This initial brightening of the discrete arc occurs at the onset of a period of intense kilometric radiation. On the following Dapp photograph, that for orbit 1100, which was taken at about 2135 UT, a moderately bright discrete arc is

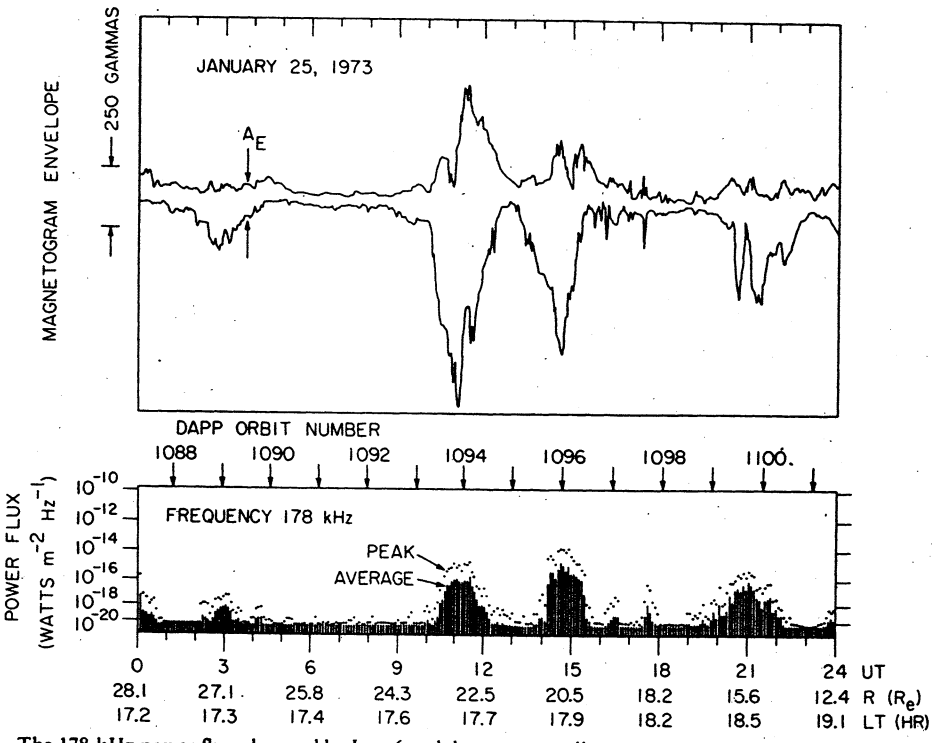

Fig. 10. The 178-kHz power flux observed by Imp 6 and the corresponding ground magnetogram envelopes for January 25, 1973. Three main periods of magnetic substorm activity occurred during this day (1000–1230 UT, 1330–1530 UT, and 1950–2300 UT), and each of these substorms is associated with a period of intense kilometric radiation.

seen, and a broad region of diffuse aurora is evident in the local midnight region. Moderately intense kilometric radiation ($\sim 10^{-16}$ W m^{-2} Hz^{-1}) is also detected by Imp 6 at this time. Both the magnetic activity and the 178-kHz power flux are decreasing, probably indicating that this photograph was obtained during the recovery phase of the substorm. On the next Dapp orbit, 1101, both the discrete aurora and the kilometric radiation have disappeared. The band of diffuse aurora is still evident, though with reduced intensity, near the bottom of the photograph for this orbit.

These data show that the kilometric radiation detected by Imp 6 is closely associated with the occurrence of aurora in the Dapp photographs. The association with aurora is in fact to be expected, since *Dunckel et al.* [1970] showed that the occurrence of kilometric radiation (referred to in their study as high-pass noise) is closely correlated with the *AE* index. However, the Imp 6/Dapp comparisons now show that the kilometric radiation is mainly associated with the discrete arcs found at high latitudes in the local evening. The kilometric radiation does not appear to be as closely associated with the diffuse aurora observed at lower latitudes near local midnight, since the diffuse aurora is sometimes evident in the Dapp photographs after the kilometric radiation has disappeared (as is true in orbits 1095 and 1101).

DISCUSSION

Substantial evidence has been presented showing that the terrestrial kilometric radiation detected by Imp 6 and 8 is generated at low altitudes ($R < 3.0\ R_E$) near the earth in association with discrete auroral arcs. Since this radio emission occurs at frequencies much greater than either the plasma frequency or the electron gyrofrequency in the outer magnetosphere, it is not surprising that the radiation is generated at relatively low altitudes, because only in this region are the characteristic frequencies of the plasma comparable to the frequency of the radiation. At low altitudes the propagation and the generation of the kilometric radiation are strongly influenced by the propagation cutoffs produced by the ionospheric plasma. Figure 13 shows a model of the expected variation of the plasma frequency f_p (proportional to the square root of the electron density) and the electron gyrofrequency f_g as a function of the geocentric radial distance for a representative auroral field line ($L = 8$). The polar ionospheric model used to compute the plasma frequency is that of *Banks and Holzer* [1969]. The electron density is given by Banks and Holzer only for $R < 2.0\ R_E$. The electron density used for $R > 2.0\ R_E$ is a qualitative extrapolation of Banks and Holzer's model to an asymptotic density of about 1 el cm^{-3} at large radial distances.

Two propagation cutoffs occur for the free-space electromagnetic modes propagating in a plasma [*Stix*, 1962]. The left-hand-polarized ordinary (L, O) mode has a cutoff at the plasma frequency f_p, and the right-hand-polarized extraordinary (R, X) mode has a cutoff at a frequency $f_{R=0}$, given by

$$f_{R=0} = (f_g/2) + [(f_g/2)^2 + f_p^2]^{1/2}$$

These propagation cutoffs are indicated by the crosshatched lines labeled (R, X) cutoff and (L, O) cutoff in Figure 13. These cutoffs represent the low-frequency limit of the electromagnetic modes that can propagate freely away from the earth and therefore are the altitude limits above which the kilometric radiation must be generated. Figure 13 shows, for example, that at a frequency of 178 kHz the minimum radial distances at which the right- and left-hand-polarized modes can propagate are about 2.5 and 1.8 R_E, respectively. At present, the polarization of the terrestrial kilometric radiation has not been determined, although such measurements are possible with the University of Minnesota plasma wave experiment

on Imp 6 (P. Kellogg, personal communication, 1973), and so the mode of propagation is not known. Since the radiation is almost certainly emitted by electrons, which rotate around the magnetic field in the right-hand sense, it is considered highly likely that the kilometric radiation is emitted in the right-hand-polarized (R, X) mode.

Regardless of the mode of propagation the observed spatial distribution of the kilometric radiation can be understood from the ray paths of the emitted radiation. Figure 14 illustrates the expected ray paths for electromagnetic waves generated at relatively low altitudes on an auroral field line. The surface labeled 'propagation cutoff surface' in this illustration is the three-dimensional surface defined by the radial distance of the propagation cutoff for a particular mode and a fixed frequency. This surface has a similar shape for both modes of propagation, and so only one cutoff surface is shown in Figure 14. At magnetic latitudes of less than about 45° the cutoff surface tends to follow the contour of the plasmasphere boundary because of the rapid increase in the plasma density (hence an increase in f_p and $f_{R=0}$) at the plasmapause. At higher latitudes (outside the plasmasphere) the cutoff surface is located at lower altitudes and is determined by the parameters of the polar ionosphere (Figure 13).

Since the index of refraction goes to zero at a propagation cutoff [*Stix*, 1962], there is a strong tendency for the ray paths to be refracted away from the cutoff surface (Figure 14). This tendency is strongest for waves generated close to the cutoff and decreases as the generation region moves to higher altitudes above the cutoff point. The general effect of this refraction, when a distribution of emitted wave normal directions is considered, is to direct the radiation into the interior of a conical region whose axis is aligned roughly normal to the propagation cutoff surface. The half angle of this cone depends strongly on the altitude of generation above the cutoff surface (Figure 14).

The observed angular distribution of the kilometric radia-

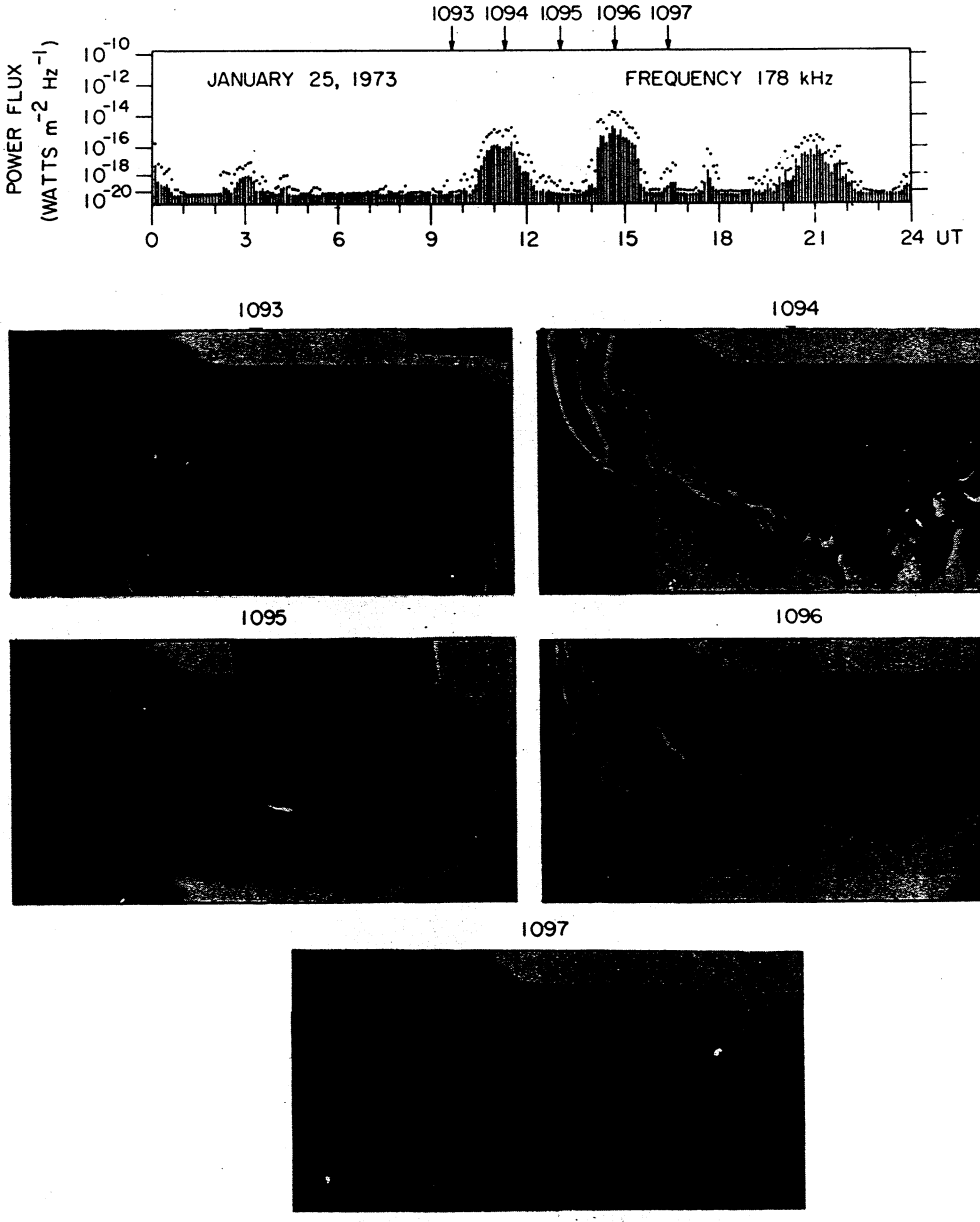

Fig. 11. The Dapp auroral photographs obtained during the first two periods of major substorm activity in Figure 10. Note that the kilometric radiation appears to be more closely related to discrete auroral arcs than to the diffuse aurora, as is true in orbit 1095, for which a diffuse aurora is present near local midnight but no kilometric radiation is evident.

tion (Figure 9) can largely be explained from the conical distribution of ray paths illustrated in Figure 14 and the spatial location of the source. It is well known that very bright discrete auroral arcs are most pronounced in the local evening [*Akasofu*, 1968; *Snyder et al.*, 1974]. If the kilometric radiation is generated by electron precipitation associated with discrete arcs in the local evening region, it is evident from the ray paths in Figure 14 that the radiation can be observed only at very high magnetic latitudes in the local morning, in agreement with the Imp 6 observations in Figure 9. In the local evening the radiation should be observed at essentially all latitudes, provided that the observing point is beyond the shadow zone produced by the plasmasphere boundary, again in agreement with the Imp 6 observations.

At a radial distance of 30 R_E the terrestrial kilometric radiation is found to have a maximum average power flux (1% occurrence) of about 10^{-14} W m^{-2} Hz^{-1} at 178 kHz. By means of this power flux and on the assumption that the effective bandwidth of the emission is 300 kHz and that the radiation is emitted uniformly over a solid angle of about 6.5 sr (estimated from Figure 9), the total power radiated is about 7.0×10^8 W. Since the solid angle used to calculate the total radiated power is based on the average solid angle at a relatively low power flux, it is possible that the instantaneous solid angle of the emitted radiation may be substantially smaller when high intensities are observed. The solid angle can be determined accurately by comparing the power flux simultaneously at two or more points. The preliminary result of comparing simultaneous Imp 6 and 8 data is that comparable peak power fluxes are observed at widely different locations, provided that both spacecraft are within the region where the radiation has a high probability of occurrence (Figure 9). These comparisons indicate that the radiation is emitted over a large solid angle event at high intensities and that the peak total power radiation is of the order of 10^9 W. Further analysis of simultaneous Imp 6 and 8 data should provide a firm determination of the total radiated power.

The maximum power dissipated by charged particles in the aurora during an auroral substorm is about 10^{11} W [*Akasofu*, 1968]. If the corresponding maximum power of the kilometric radiation is 10^9 W, then the efficiency with which this radiation is generated must be about 1%. From all present knowledge of magnetospheric radio emissions the generation of terrestrial kilometric radiation represents a very efficient conversion of charged-particle energy into radio emission.

Since electromagnetic radiation occurs above the plasma frequency in a wide variety of physical situations, for example, in type 3 solar radio noise bursts [*Wild*, 1950] and in Jovian decametric radiation [*Warwick*, 1967], it is of considerable

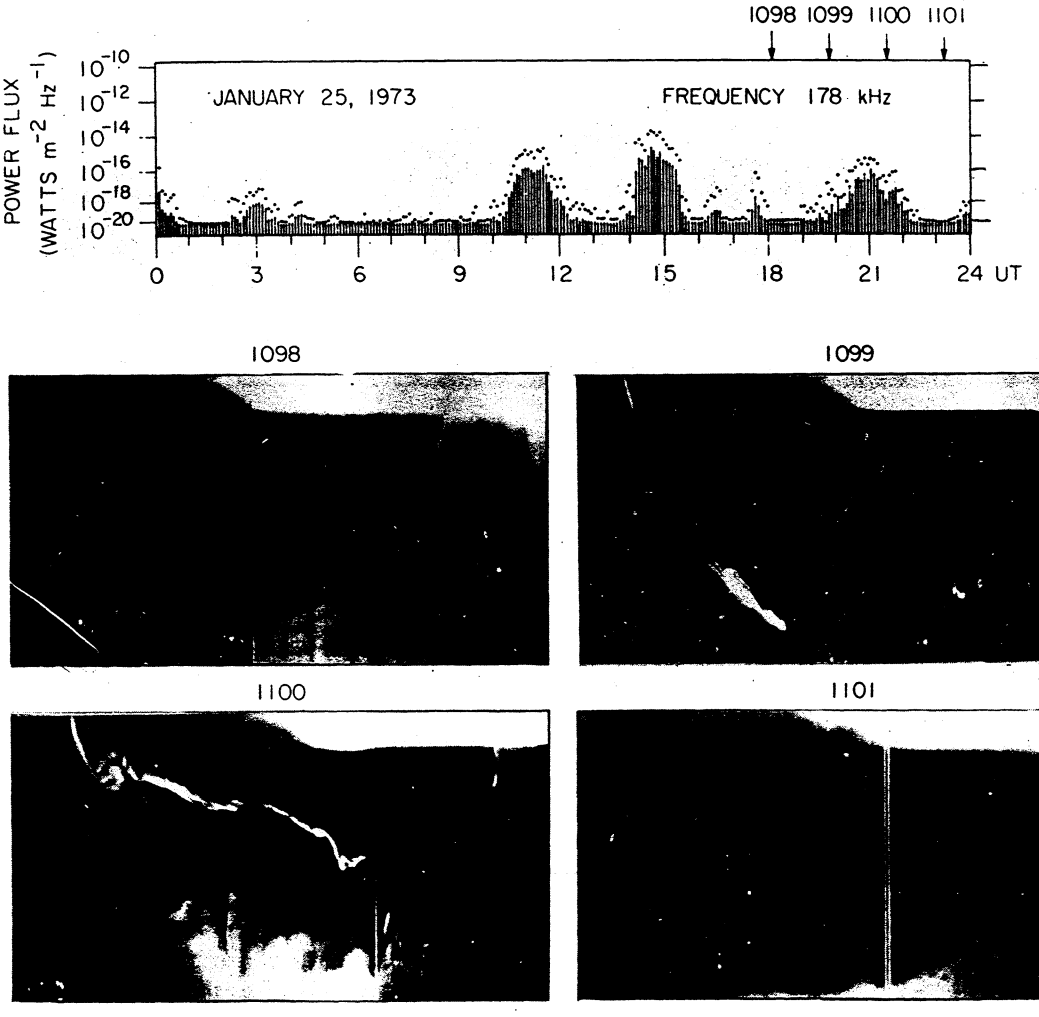

Fig. 12. The Dapp auroral photographs obtained during the third period of major substorm activity in Figure 10. Note orbit 1099, which shows the onset of a discrete auroral arc at the time when the kilometric radiation is just beginning.

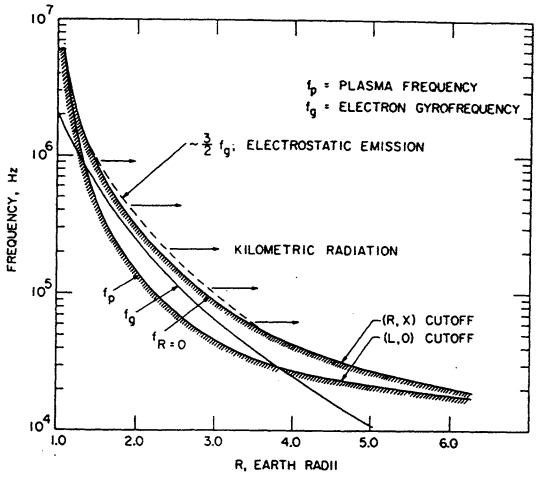

Fig. 13. Polar ionospheric model showing the expected radial variation of the cutoff frequencies f_p and $f_{R=0}$ for the left- and right-hand-polarized free-space electromagnetic modes. The upper- and lower-frequency limits of the terrestrial kilometric radiation can be explained if the radiation is generated by coherent cyclotron radiation from energetic auroral electrons.

general interest to establish the origin of the terrestrial kilometric radiation. In this case it should be possible to make considerable progress toward identifying the basic mechanism involved, since a great deal is known about the electron energy distribution and intensities associated with auroral arcs and about the basic plasma parameters in the generation region. Discrete auroral arcs have been directly associated with intense 'inverted V' electron precipitation bands observed by low-altitude polar-orbiting satellites [*Frank and Ackerson*, 1971; *Ackerson and Frank*, 1972]. Because of the observed association between the terrestrial kilometric radiation and discrete auroral arcs it is almost certain that the energetic electrons in these inverted V events are directly responsible for the kilometric radiation. The inverted V electron precipitation events have fluxes of up to 10^9 el cm^{-2} s^{-1} sr^{-1} and maximum energies of about 10 keV. Detailed energy spectra for these events are given by *Frank and Ackerson* [1971].

Two general mechanisms can be considered to explain the generation of the terrestrial kilometric radiation: (1) the noise may be generated by incoherent radiation from energetic electrons, or (2) the noise may be generated by a coherent plasma instability. Because of the very high efficiency with which the kilometric radiation is generated it is considered very unlikely that this noise is produced by an incoherent mechanism. A rough calculation shows that the power radiated by incoherent cyclotron radiation from energetic auroral electrons is too small by a factor of about 10^8. Similarly, the power radiated by incoherent Cerenkov radiation [*Taylor and Shawhan*, 1974] and by incoherent gyrosynchrotron radiation [*Frankel*, 1973] appears to be much too small to account for the observed intensities of the kilometric radiation.

What is needed to explain the terrestrial kilometric radiation is a suitable mechanism for providing coherence between the radiating electrons in order to increase the radiated power (by a factor of N^2, where N is the number of electrons that are moving in phase). Recently, to explain the Jovian decametric radiation, which may in fact be very similar to the terrestrial kilometric radiation, *Scarf* [1973] has suggested that a purely electrostatic plasma instability that occurs at a frequency of about $3f_g/2$ may organize the phase of the energetic electrons in the Jovian magnetosphere, thereby greatly increasing the power radiated by these electrons. This same mechanism had also been proposed by *Gurnett and Shaw* [1973] to explain the generation of electromagnetic waves trapped in the magnetosphere above the local plasma frequency. It is not known whether electrostatic emissions at $3f_g/2$ actually occur in the region where the kilometric radiation is generated, because Imp 6 does not go through this region (see the trajectory in Figure 8, for example). However, these electrostatic emissions do occur over large regions of the magnetosphere [*Kennel et al.*, 1970] and are expected in regions of field-aligned currents associated with discrete auroral arcs. If the kilometric radiation is generated at $3f_g/2$ by this mechanism, then a simple explanation arises for the observed bandwidth of the radiation. Figure 13 shows that the right-hand-polarized free-space mode cannot propagate at a frequency less than the (R, X) cutoff at $f_{R=0}$. If the radiation is emitted as right-hand-polarized electromagnetic waves at $3f_g/2$, then this radiation can only propagate away from the generation region in a limited frequency range, from about 50 kHz to 1.2 MHz for the model in Figure 13.

To explain the intense decametric radio emissions associated with Jupiter's moon Io, *Goldreich and Lynden-Bell* [1969] have proposed a coherent cyclotron mechanism for directly generating intense electromagnetic radiation from a beam of weakly relativistic electrons. This mechanism may also be able to account for the main characteristics of the terrestrial kilometric radiation, since many similarities exist between the terrestrial kilometric radiation and the Jovian decametric radiation. These similarities include the following:

1. In both cases the radiation appears to be associated with magnetic field–aligned beams of electrons with energies of the order of tens of keV.
2. In both cases the frequency of the radiation appears to be closely associated with the electron gyrofrequency (hence the magnetic field strength) in the emitting region.

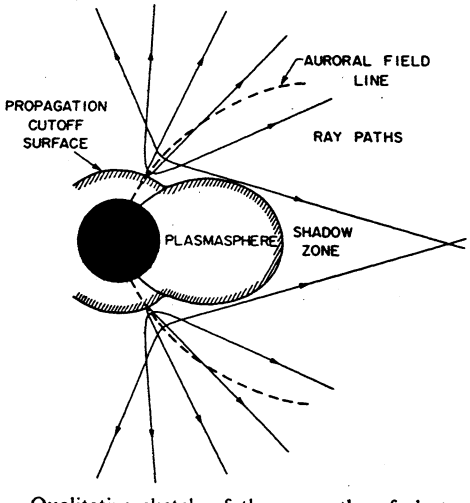

Fig. 14. Qualitative sketch of the ray paths of electromagnetic radiation emitted at low altitudes and fixed frequency along an auroral field line. Because the refractive index goes to zero at the propagation cutoff, there is a strong tendency for the ray paths to be refracted upward, away from the propagation cutoff surface. The propagation cutoff surfaces for the (R, X) and (L, O) modes are similar, and so only one surface is shown. The shadow zone caused by the plasmasphere accounts for the low-latitude cutoff evident in Figure 7. Also, note that radiation from the local evening can reach the local morning only at very high magnetic latitudes, in agreement with the observed angular distribution in Figure 9.

3. In both cases the angular distribution of the emitted radiation is associated with a distinct cone-shaped boundary that is at a large angle to the magnetic field direction in the emitting region.

4. In both cases the total emitted power (10^9 W and 2×10^7 W) and field-aligned currents (10^6 A in both cases) are quantitatively similar.

It is interesting to note that the coherent cyclotron mechanism could also account for the primary frequency range of the kilometric radiation, since the resonance energy at which the emission occurs decreases rapidly as the ratio of the electron plasma frequency to electron gyrofrequency, f_p/f_g, decreases (S. Shawhan, personal communication, 1974). On the assumption that the number of electrons in the auroral electron beam increases with decreasing energy, the maximum growth rate, and hence the intensity, occurs where the ratio f_p/f_g is a minimum; this is at a frequency of about 150 kHz for the ionospheric model used in Figure 13.

Acknowledgments. I wish to extend my special thanks to S.-I. Akasofu, who provided the magnetogram records used in this study and to W. S. Kurth and R. R. Anderson, who assisted in the data analysis. The Dapp photographs were provided by the NOAA World Data Center. This work was supported in part by NASA under contracts NAS5-11074 and NAS5-11431 and grant NGL-16-001-043 and by the Office of Naval Research under grant N00014-68-A-0196-0009.

* * *

The Editor thanks R. E. Barrington and N. Dunckel for their assistance in evaluating this paper.

REFERENCES

Ackerson, K. L., and L. A. Frank, Correlated satellite measurements of low-energy electron precipitation and ground-based observations of a visible auroral arc, *J. Geophys. Res., 77,* 1128, 1972.

Akasofu, S.-I., *Polar and Magnetospheric Substorms,* p. 223, D. Reidel, Dordrecht, Netherlands, 1968.

Banks, P. M., and T. E. Holzer, High-latitude plasma transport: The polar wind, *J. Geophys. Res., 74,* 6317, 1969.

Brown, L. W., The galactic radio spectrum between 130 kHz and 2600 kHz, *Astrophys. J., 180,* 359, 1973.

Dunckel, N., B. Ficklin, L. Rorden, and R. A. Helliwell, Low-frequency noise observed in the distant magnetosphere with Ogo 1, *J. Geophys. Res., 75,* 1854, 1970.

Frank, L. A., and K. L. Ackerson, Observations of charged-particle precipitation into the auroral zone, *J. Geophys. Res., 76,* 3612, 1971.

Frankel, M. S., LF radio noise from the earth's magnetosphere, *Radio Sci., 8,* 991, 1973.

Goldreich, P., and D. Lynden-Bell, Io, A Jovian unipolar inductor, *Astrophys. J., 156,* 59, 1969.

Gurnett, D. A., and R. R. Shaw, Electromagnetic radiation trapped in the magnetosphere above the plasma frequency, *J. Geophys. Res., 78,* 8136, 1973.

Kennel, C. F., F. L. Scarf, R. W. Fredricks, J. H. McGehee, and F. V. Coronitti, VLF electric field observations in the magnetosphere, *J. Geophys. Res., 75,* 6136, 1970.

Scarf, F. L., A new model for the high-frequency decametric radiation from Jupiter, *Rep. 24876-6001-RU-00,* 8 pp., TRW Syst. Group, Redondo Beach, Calif., 1973.

Snyder, A. L., S.-I. Akasofu, and T. N. Davis, Auroral substorms observed from above the north polar region by a satellite, *J. Geophys. Res., 79,* 1393, 1974.

Stix, T. H., *The Theory of Plasma Waves,* p. 27, McGraw-Hill, New York, 1962.

Taylor, W. W. L., and S. D. Shawhan, A test of incoherent Cerenkov radiation for VLF hiss and other magnetospheric emissions, *J. Geophys. Res., 79,* 105, 1974.

Warwick, J., Dynamic spectra of Jupiter's decametric emission, 1961, *Astrophys. J., 137,* 41, 1963.

Warwick, J. W., Radiophysics of Jupiter, *Space Sci. Rev., 6,* 841, 1967.

Wild, J. P., Observations of the spectrum of high-intensity solar radiation at meter wavelengths, 3, Isolated bursts, *Aust. J. Sci. Res., Ser. A, 3,* 541, 1950.

(Received February 14, 1974;
accepted June 21, 1974.)